Lateral Manipulation of Atomic Vacancies in Ultrathin Insulating Films

Zhe Li,[†] Hsin-Yi Tiffany Chen,[‡] Koen Schouteden,[†] Koen Lauwaet,[†] Ewald Janssens,[†] Chris Van Haesendonck,[†] Gianfranco Pacchioni,[*,‡] and Peter Lievens[*,†]

[†]Laboratory of Solid-State Physics and Magnetism, KU Leuven, Celestijnenlaan 200 d, Box 2414, BE-3001 Leuven, Belgium and [‡]Dipartimento di Scienza dei Materiali, Università di Milano-Bicocca, Via Cozzi 55, I-20125 Milano, Italy

ABSTRACT During the last 20 years, using scanning tunneling microscopy (STM) and atomic force microscopy, scientists have successfully achieved vertical and lateral repositioning of individual atoms on and in different types of surfaces. Such atom manipulation allows the bottom-up assembly of novel nanostructures that can otherwise not be fabricated. It is therefore surprising that controlled repositioning of virtual atoms, *i.e.*, atomic vacancies, across atomic lattices has not yet been achieved experimentally. Here we use STM at liquid helium temperature (4.5 K) to create individual Cl vacancies and subsequently to laterally manipulate them across the surface of ultrathin sodium chloride films. This allows monitoring the interactions between two neighboring vacancies with different separations. Our findings are corroborated by density functional theory calculations and STM image simulations. The lateral manipulation of atomic vacancies opens up a new playground for the investigation of fundamental physical properties of vacancy nanostructures of any size and shape and their coupling with the supporting substrate, and of the interaction of various deposits with charged vacancies.

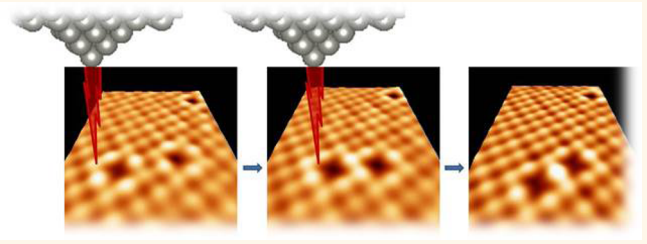

KEYWORDS: lateral vacancy manipulation · scanning tunneling microscope · density functional theory · vacancy–vacancy interaction · ultrathin insulating films

Vacancies are known to exist in all sorts of materials, and they already have been widely investigated ranging from atomic vacancies to vacancy islands for various metal, semiconductor, and insulator surfaces. Color and luminescence can be induced in insulators by creating atomic vacancies.[1] Vacancies are also known to strongly affect doping processes in semiconductors, which is in particular the case for oxide semiconductors such as ZnO.[2] Vacancies are also important for surface reactivity. Oxygen vacancies in metal oxide surfaces play, for example, an important role in promoting the rate of surface electrochemical incorporation reactions.[3] Vacancies in surfaces can also affect diffusion of adsorbed particles. Vacancies in insulating surfaces have been used for trapping molecules[4] and nanoclusters.[5] Vacancies can also trap different amounts of electrons and hence can have different charge states.[6,7] It has been demonstrated that when a supported Au cluster binds to a charged O vacancy on a MgO surface, it can become chemically active due to electron transfer from the vacancy to the adsorbed cluster.[8,9] On the other hand, large vacancy aggregates such as vacancy islands in metal surfaces have been investigated, revealing quantum size effects due to surface state confinement in the vacancy islands.[10,11]

Vacancies can be investigated reliably at the atomic level using scanning tunneling microscopy (STM) and spectroscopy (STS).[10,12] Moreover, these techniques also allow locally creating atomic vacancies with the STM tip. It has been demonstrated that Cl vacancies can be created in thin NaCl films either by electron-stimulated desorption[13] or by bringing the STM tip into contact with the NaCl surface.[14] The latter method results in a single Cl vacancy at the location of the tip approach and at the same time in a chemically functionalized STM tip[14] that is very well suited for atomic-resolution investigation of nanoparticles.[15] Yet, this approach is less optimal for STM tip manipulation experiments and spectroscopy investigations due to the limited stability. The former method typically produces one up to a few atomic Cl vacancies near the location of the electron-stimulated desorption and leaves the bare

* Address correspondence to gianfranco.pacchioni@unimib.it, peter.lievens@fys.kuleuven.be.

Received for review February 5, 2015 and accepted March 13, 2015.

Published online March 13, 2015
10.1021/acsnano.5b00840

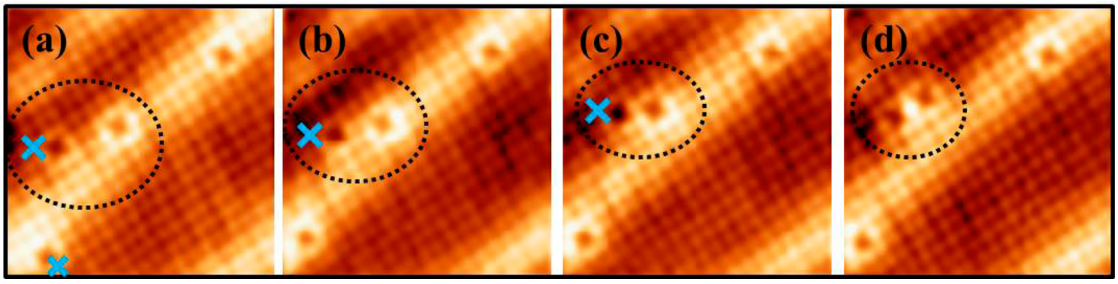

Figure 1. Lateral manipulation of previously created Cl vacancies in 2L NaCl/Au(111) by locally applying a voltage pulse with the STM tip. (a−d) 6.5 × 6.5 nm^2 atomic-resolution STM topography images of Cl vacancies in 2L NaCl recorded at V = 1 V, I = 0.2 nA. The black dotted ellipse indicates the vacancies that are involved in the dimer formation. Note that when comparing (b) to (a), the vacancy in the bottom-left corner in (a) is also moved because an additional intentional manipulation step is performed for this vacancy. The blue crosses in (a)−(c) indicate the locations where voltage pulses are applied to manipulate the vacancies.

metal STM tip unaffected. Cl vacancies in NaCl films on Cu substrates have previously been studied as an interesting model system for investigating the strong electron−phonon (*e*−ph) coupling between a localized vacancy state (VS) and the optical phonons in a polar insulator,[16] while the positive charge of the Cl vacancy is confirmed by observation of interface-state localization (ISL) at the vacancy site. Recently, it has been reported that the local thickness of thin NaCl insulating films grown on Cu(111) can be determined by measuring the lifetime of the VS of single Cl vacancies.[17]

Since vacancies play a key role in the local properties of a material, controlled manipulation of these virtual atoms is of great interest, as it allows repositioning them to a desired location or allows them to form artificial functional vacancy aggregates. For example, atomic patterns of dangling bonds induced by H vacancies on semiconducting surfaces can be controllably created by desorption of the H atoms.[18,19] These structured dangling bonds can be promising candidates for charge qubits[20] and can also be used for chemisorption of molecules such as I_2[21] and HCl.[22] Controllable manipulation of adatoms, molecules, nanoclusters, and dopants has already been achieved on/in surfaces of metals, semiconductors, and insulators.[5,23−29] However, while controlled lateral manipulation of individual vacancies across a surface lattice has been predicted theoretically to be possible using an atomic force microscope,[30] it has not been achieved experimentally.

Here we demonstrate for the first time that Cl vacancies created in atomically thin NaCl films on Au(111) can be laterally moved with the STM tip. By combining STM/STS measurements and DFT calculations, we elucidate that the Cl vacancies are positively charged (F^+ center). The VS and the localized interface state (IS), which are associated with the vacancy, are both found to shift toward lower energy upon the formation of a vacancy dimer. Mutual interaction between two neighboring vacancies leads to the formation of a symmetric and an antisymmetric VS in the vacancy dimer. Moreover, the coupling between the VS and the optical phonons in the NaCl film is shown to be reduced for the vacancy dimer compared to the individual vacancy.

RESULTS

Creation and Lateral Manipulation of Cl Vacancies in 2L NaCl. Figure 1a presents a typical STM topography image of several atomic vacancies that are created by electron-stimulated desorption. This is achieved by retracting the tip away from the surface and applying a voltage pulse, typically in the range from 8 to 8.5 V. The voltage pulse must be well above the energy of the bottom of the conduction band of the NaCl film, such that electrons can effectively tunnel *into* the NaCl film (rather than tunneling *through* it to the Au(111) substrate) and thereby stimulate the Na and Cl ions. To avoid excessive surface damage by the high-voltage pulse (typically above 8.5 V), the tip is initially retracted as far as 3 nm, and next the tip−sample distance is gradually reduced until a vacancy can be created by a voltage pulse. Note that the precise distance varies from tip to tip, since the shape of the tip determines the effective electric field experienced by the surface. Since only the Cl ions are imaged as protrusions in the STM topography images when using a metallic STM tip,[31] the created vacancies in Figure 1a can be assigned as Cl vacancies. In STM topography images the Cl vacancy appears as a missing protrusion where the four nearest-neighbor Cl ions are slightly elevated. Similar observations have been reported before for single Cl vacancies in NaCl films on copper surfaces.[13,16]

By retracting the STM tip around 2 nm from the surface and applying a positive voltage pulse around 7.5 V (*i.e.*, below the voltage used for vacancy creation) near an already created Cl vacancy, the vacancy can be moved to its neighboring Cl site, away from the location where the voltage pulse was applied. The vacancy can be considered a virtual atom that has a positive charge, as will be discussed below. When the STM tip applies a positive voltage pulse near the virtual atom, the virtual atom experiences a repulsive force that can

move the vacancy away from the tip. In the migration process of a Cl vacancy, a nearest-neighbor Cl ion jumps into the original vacant site, leaving a new vacancy behind. As illustrated in Figure 1a–c, when applying a voltage pulse at the blue cross on the left-hand side of the vacancy within the dotted ellipse, the vacancy moves to the right. Alternatively, this corresponds to a Cl ion that moves to the left. Since the Cl ion has a negative charge and the applied voltage is positive, the applied voltage pulse on the left-hand side of a vacancy attracts another nearest-neighbor Cl ion, thereby annihilating the target vacancy site and leaving a vacancy on the right. As a result, the vacancy moves to the right. This way, the two Cl vacancies indicated by the black dotted ellipse in Figure 1a can be moved closer to each other step by step (Figure 1b), allowing the formation of so-called vacancy dimers with separation distances of 0.89 ± 0.02 nm (Figure 1c, hereafter referred to as dimer I) and 0.80 ± 0.02 nm (Figure 1d, hereafter referred to as dimer II). The distance between two vacancies is determined based on our experimentally measured nearest-neighbor Cl–Cl distance of 0.40 ± 0.02 nm of the NaCl film on Au(111). In our experiments it was not possible to form a vacancy dimer where the two constituting vacancies are not separated by at least one Cl ion, which implies that either such vacancy dimers are not stable or their formation involves a higher energy barrier. Larger vacancy nanostructures consisting of up to three and four atomic Cl vacancies were created as well and are presented in Figure S1 in the Supporting Information (SI). The vacancies in these larger nanostructures are all separated by at least one Cl ion.

We note that in our manipulation approach the tip is retracted relatively far away from the surface, which implies that the applied voltage pulse to the target vacancy has an intrinsic finite "spatial extent" (typically within a radius of about 1.2 nm) and hence can also affect the vacancies that are located nearby (see, *e.g.*, Figure S1b and the corresponding discussions in the SI). The presence of nearby vacancies does not affect the tunneling settings required to move the targeted vacancy. We here must emphasize that the unintended movement of vacancies near the target vacancy is a very local effect. In particular, when the vacancies are further separated from each other, *i.e.*, typically more than about 1.2 nm, there are no unintended movements.

The thickness of the NaCl film appears to be crucial for successful Cl vacancy creation and manipulation. For 3L NaCl Cl vacancies can be created by electron-stimulated desorption using a smaller voltage pulse (typically above 6 V) when compared to 2L NaCl, while it is also possible to damage the 3L NaCl surface when the voltage pulses exceed 6 V. On the other hand, for 1L NaCl vacancies cannot be created by electron-stimulated desorption using voltage pulses as large as 10 V. This indicates that the NaCl film becomes less resistant against vacancy formation with increasing film thickness: 1L NaCl seems to be not affected by the high-voltage pulse, while 3L NaCl is too sensitive to the high-voltage pulse. For both 1L and 3L NaCl we have not been able to move the vacancies using the approach described above. Therefore, in the following we focus on the Cl vacancies in 2L NaCl on Au(111).

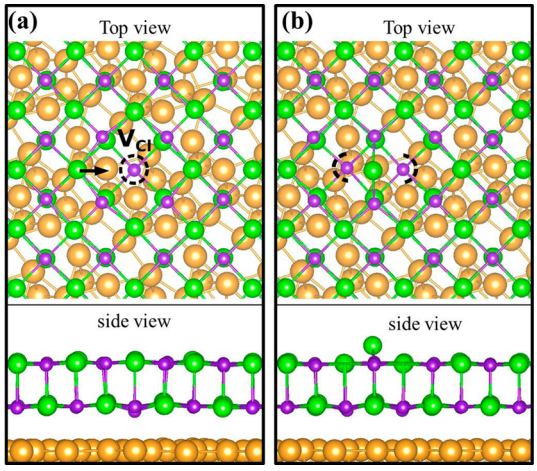

Figure 2. Computed structures of (a) the initial state and (b) the transition state (TS) of a Cl vacancy migrating in a 2L NaCl/Au(111) film. Violet, green, and gold spheres refer to Na, Cl, and Au atoms, respectively. The arrow in (a) indicates this Cl atom moves to the TS in (b). The Cl atom and the vacancy move in opposite directions. The dashed circle and half circles in (a) and (b), respectively, indicate the position of the Cl vacancies.

Energy Barrier for Cl Vacancy Migration. The transition state for Cl vacancy migration (Cl diffusion) was searched for by first-principles calculations using constrained optimization and the dimer method, a procedure designed for automatic search for transition states.[32] First, an initial Cl vacancy is created by removing a neutral Cl atom from the 2L NaCl/Au(111) (see Figure 2a). On an unsupported 2L NaCl slab this would result in a neutral F^0 paramagnetic center with one electron trapped in the cavity. On the 2L NaCl/Au(111) surface the electron trapped in the vacancy is unstable and is transferred to the Au(111) support, formally resulting in a F^+ center with no electrons trapped in the vacancy.

Cl vacancy migration is accomplished by moving a nearest-neighbor Cl atom to the Cl vacancy position. In the transition state (TS) (see Figure 2b) the diffusing Cl atom is found to be 0.11 nm above the NaCl surface and equidistant from the two vacancies. Both the constrained optimization and the dimer method predict an energy barrier of 0.58 eV. Unfortunately it is not possible to derive a meaningful energy barrier value from our experiments that can be directly compared to the calculated energy barrier. It is however obvious that the applied voltage pulse induces an energy gain for the Cl ions below the STM tip apex. Since the electric field under an STM tip crucially depends on the precise shape of the tip apex[33] (which is not known in our experiment), we consider a simple electrostatics-based

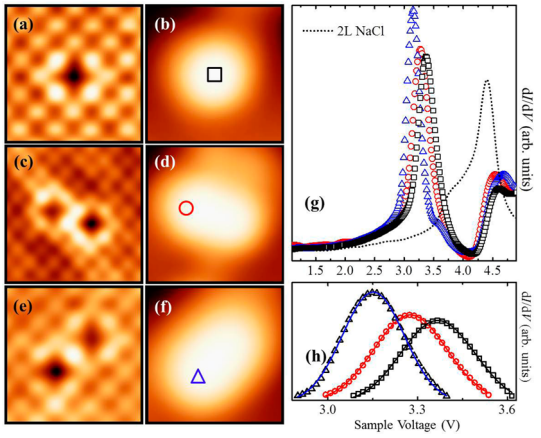

Figure 3. (a and b) 2.2 × 2.2 nm^2 STM topography images of a single Cl vacancy in 2L NaCl recorded at V = 1.00 and 3.35 V, respectively. (c) and (d) 3.0 × 3.0 nm^2 STM topography images of dimer I in 2L NaCl recorded at V = 1.00 and 3.30 V, respectively. (e and f) 2.2 × 2.2 nm^2 STM topography images of dimer II in 2L NaCl recorded at V = 1.00 and 3.15 V, respectively. (g) dI/dV spectra taken on bare 2L NaCl (black dotted line), an individual Cl vacancy (black squares), one of the vacancies of dimer I (red circles), and one of the vacancies of dimer II (blue triangles). The recorded locations are indicated in (b), (d), and (f). (h) Background-corrected dI/dV spectra of the VSs in (g), fitted to Gaussian line shapes (solid lines). The spectra are corrected by subtracting the spectrum of bare 2L NaCl.

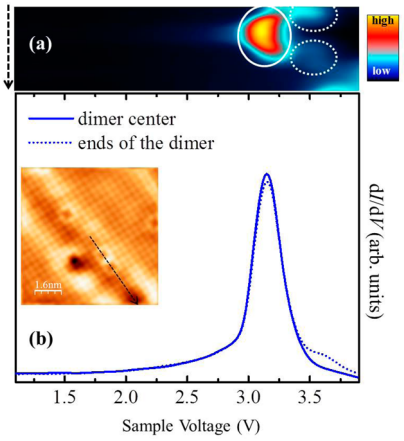

Figure 4. (a) 5 V × 5 nm color visualization of (dI/dV)(V) spectra taken along the black dotted lines in the inset of (b). The solid and dotted white ellipses indicate symmetric and antisymmetric states, respectively. (b) Single-point dI/dV spectra taken in the center (solid blue curve) and on one of the vacancies (dotted blue curve), respectively, of the vacancy dimer II.

approximation, *i.e.*, treating the tip−sample junction as two parallel plates: the potential energy $U = qV$, where q is the charge of the tunneling electrons. Assuming q = 1e, V = 0.58 V is needed to reach the TS. The tip height for an experimental voltage pulse of 7.5 V should be (7.5 eV/0.58 eV × 0.11 nm =) 1.4 nm, which is consistent with retracting the STM tip by 2 nm from the surface in the experiment. We note that this very simple electrostatics-based model is only one of the possible rationales.

DISCUSSION

Vacancy State Interactions. Figure 3a, c, and e present STM topography images of an individual vacancy (F^+ center) and of two vacancy dimers (M^{2+} centers, *i.e.*, dimer I and dimer II) with different separation distances that are formed by lateral manipulation in 2L NaCl(100)/Au(111) as described above.

While an individual Cl vacancy is observed as a depression (missing protrusion) at low voltages (Figure 3a), it is revealed as a bright protrusion (Figure 3b) at the high unoccupied state level. This remarkable change of appearance can be related to the presence of the VS. The VS appears as a pronounced unoccupied state around 3.35 eV in the dI/dV spectrum taken on an individual Cl vacancy (black squares in Figure 3g). For comparison we also present a reference spectrum of the bare 2L NaCl film (black dotted line in Figure 3g). This reference spectrum reveals two resonances around 3.7 eV (shoulder peak) and 4.4 eV (main peak), which are related to the Au bulk band gap edge[34] and the first image-potential state (IPS) of the 2L NaCl film,[35] respectively. Following the recent work reported in ref 36, the onset of the conduction band of the 2L NaCl is likely to be hidden in the IPS resonances. Within the accuracy of our experiments, the peak position of the VS in the dI/dV spectra in Figure 3 is the same for all single vacancies, *i.e.*, independent of the surface reconstruction of the underlying Au(111) surface.

Upon moving the two vacancies toward each other with the STM tip, we find that the VS shifts toward lower energies. For dimer I (Figure 3c) the VS is located at a lower energy around 3.3 eV (red circles in Figure 3g). For dimer II the main resonance is shifted further downward to 3.15 eV. Interestingly, a shoulder peak can be observed around 3.57 eV, indicative of splitting of the VS. These observed shifts and splitting of the VS can be related to the interactions between the constituting vacancies. The spatially extended wave functions of the VSs start to overlap with each other if the two vacancies are brought close together, which allows their interaction. Figure 4 presents the spectra taken along another vacancy dimer II. In the center of the two vacancies there appears only one state in the dI/dV spectra, while on the two ends of the dimer two states are observed (Figure 4b). The spatially resolved dI/dV spectra (Figure 4a) reveal that the two VSs form a symmetric (indicated by the solid ellipse) and an antisymmetric state (indicated by the dotted ellipses) due to the interaction between the two vacancies, which is also confirmed by the DFT calculations as described below. While the vacancy dimers are imaged as two missing protrusions (Figure 3c and e) at low voltages, they appear as one pronounced ellipsoidal protrusion (Figure 3d and f) at high voltages near the VS energy rather than as two separate protrusions.

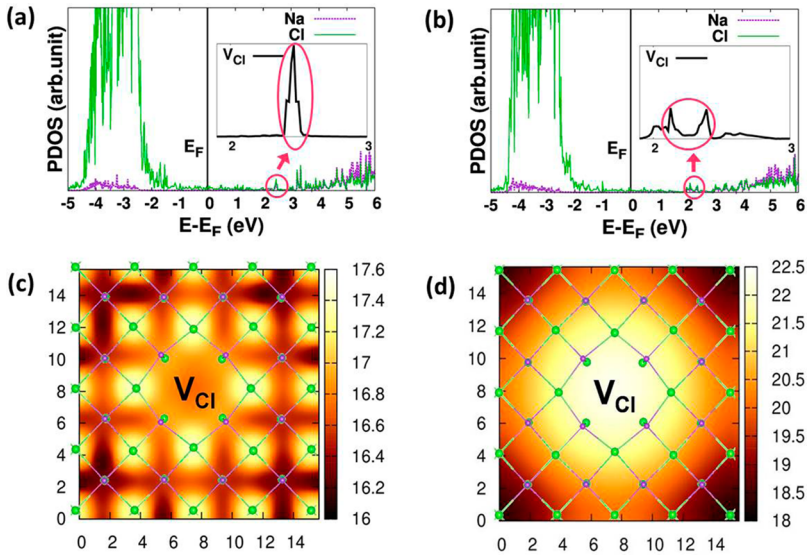

Figure 5. Projected DOS (PDOS) of a Cl vacancy (V_{Cl}) for (a) $NaCl_{1-x}$/Au(111) (F^+ center) and (b) $NaCl_{1-2x}$/Au(111) (M^{2+} center, vacancy dimer II). The insets in (a) and (b) are the local DOS (LDOS) for the F^+ and M^{2+} center, respectively. (c and d) Simulated STM images with electron density of 8×10^{-5} |e|/Å^3 of a F^+ center: (c) at low positive energy range (0−0.6 eV), (d) at high positive energy range (2.3−2.6 eV). In (c) and (d) the values of the abscissa and ordinate give the dimension (in Å), and the intensity bar at the right indicates the height (in Å) at which the electron density equals 8×10^{-5} |e|/Å^3 (the bottom of the model is set as 0 Å). Violet and green spheres in the superimposed lattices refer to Na and Cl atoms, respectively.

Height profiles of the two vacancy dimers and a single vacancy are presented in Figure S2 in the SI.

To elucidate the different appearances of the vacancy at different voltages and the role of the VS therein, we performed DFT calculations and simulations of STM images. Figure 5 presents the simulated projected (PDOS) and local density of states (LDOS) of a F^+ center and a M^{2+} center (dimer II) as well as the simulated STM image of a F^+ center in a 2L NaCl/Au(111) film at low and high voltage.

For the F^+ center the PDOS in Figure 5a reveals that an empty state arises around 2.46 eV in the band gap of the 2L NaCl. This state can be assigned as the VS of the F^+ center (the low value when compared to the experiment is due to an underestimation of the NaCl band gap in DFT calculations). A plot of the LDOS at the vacancy site (inset in Figure 5a) reveals that the peak at 2.46 eV indeed stems from the F^+ center. This is visualized in the partial charge density map at 2.46 eV in Figure S3b, which shows that the charge density is localized at the Cl vacancy site. The localized character of the VS is also evidenced in simulated STM topography images. Moreover, the simulated images confirm that the VS makes the vacancy appear as a protrusion in the STM image at high voltage (Figure 5d), while the vacancy appears as a missing protrusion at low voltage (Figure 5c), in agreement with the experiments (Figure 3a and b).

For the M^{2+} center (dimer II) the DFT calculation gives two empty states at 2.13 and 2.39 eV in the PDOS (Figure 5b). The LDOS (inset in Figure 5b) and the localized charge density at the Cl vacancy site for the two states (Figure S3d) confirm that these two states can be interpreted as VSs. The splitting of the single state of the F^+ center in two states for the M^{2+} center originates from the interaction of the two vacancies. The separation of the symmetric and antisymmetric states by 0.26 eV is in good agreement with our experimental observations (Figure 4). The shift of the two VSs toward lower energy for the M^{2+} centers when compared to the VS of the F^+ center is also consistent with the experimental observations (Figure 3g and h) and indicates that the potential created by the dimer vacancy is more attractive than for a single vacancy. Note that for dimer I, in the experiments (Figure 3c) we observe only one peak in the d*I*/d*V* spectra (Figure 3g), while the simulation reveals two states with a smaller separation (data not shown) than dimer II. This discrepancy can be attributed to the strong *e*−ph interaction that broadens the peaks in experimental d*I*/d*V* spectra (as discussed below). Consequently, for dimer I it is experimentally not possible to resolve the relatively small energy separation between the two states that are revealed in the simulation.

Figure 3h presents the vacancy d*I*/d*V* spectra of Figure 3g after subtracting the background d*I*/d*V* spectrum of the bare NaCl. These background-corrected spectra can be fitted well by a Gaussian line shape. The strong *e*−ph coupling in the tunneling through the VS gives rise to a significant broadening of spectroscopic features.[16,37] The full width at half-maximum (fwhm) of the spectra has been previously shown to be proportional to the strength of the *e*−ph coupling.[16] From the fits in Figure 3h, we find that the fwhm for the vacancies in dimer I and dimer II is smaller than that for an individual vacancy, which indicates that the *e*−ph coupling is reduced by the interaction

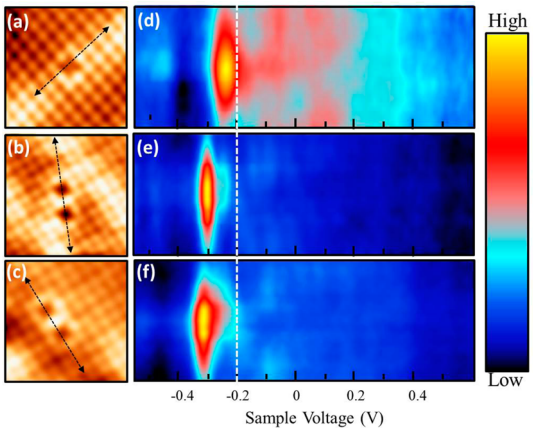

Figure 6. STM topography images of (a) an individual Cl vacancy, (b) a vacancy dimer I, and (c) a vacancy dimer II in 2L NaCl/Au(111). (d−f) 1.2 V × 4.2 nm color visualization of (d*I*/d*V*)(*V*) spectra taken along the black dotted lines in (a−c), respectively. The white dashed lines in (d−f) indicate the maximum position of the peak/step in the IS d*I*/d*V* spectra in the *hcp* and herringbone regions on the defect-free 2L NaCl/Au(111) surface.

between two neighboring vacancies. Our findings illustrate that lateral manipulation of vacancies allows monitoring the modified VS as well as the coupling between the VS and the optical phonons in the NaCl film, which contains specific vacancy nanostructures.

Localized Interface-State Interactions. Upon adsorption of the NaCl layer, the Au(111) Shockley surface state becomes an interface state at the NaCl/Au(111) interface. The IS maximum in the d*I*/d*V* spectra varies for different Au(111) surface reconstruction regions, *i.e.*, *hcp* and *fcc* regions that are separated by the herringbones. Specifically, d*I*/d*V* spectra taken on the *fcc* regions show the maximum position around −150 meV, while the spectra on both *hcp* and herringbone regions show the maximum around −200 meV.[38] Below we focus on the vacancies in the *hcp* and herringbone regions, since the observations for vacancies in *fcc* regions are qualitatively the same. In addition to the VS that exists at high energies, the Cl vacancies are also found to induce a pronounced localization of the 2L NaCl/Au(111) IS at lower energies near the Fermi level.

For an individual vacancy (in the herringbone region) (Figure 6a) and two vacancy dimers (in the *hcp* region) (Figure 6b and c) in 2L NaCl/Au(111), spatial distributions of the IS are presented in Figure 6d−f. The peak position (around −200 meV) of the IS d*I*/d*V* spectra on defect-free *hcp* and herringbone regions is indicated by a white dashed line. We find that an individual vacancy localizes the IS around −220 meV (Figure 6d). The existence of interface-state localization below the band bottom of the IS indicates that the Cl vacancies are positively charged, in agreement with our DFT calculations described above. The attractive potential resulting from the creation of the vacancy gives rise to a localized state that is split off from the IS band. Localization of surface states is also a well-known phenomenon for adatoms on bare metal surfaces.[39−41]

Unlike the VS in Figure 3, the ISL effect is not visible in the STM topography images; that is, the vacancy still appears as a missing protrusion at −220 meV (Figure 6a). After moving another vacancy nearby with the STM tip, the IS is found to be localized around −300 meV for the vacancy dimer I (Figure 6e) and around −310 mV for dimer II (Figure 6f). The localized IS is thus shifted toward lower energies by 80 or 90 mV for the vacancy dimers relative to the localized IS for a single vacancy. Since the Cl vacancies are positively charged as we have found above, the observed different energy shift of the localized IS toward lower energies may be related to an increase of the charge potential when two charged vacancies become closer to each other. A smaller ISL shift of 50 mV to lower energy on 2L NaCl/Cu(111) has been reported for a Cl vacancy dimer with a larger separation distance of 1.17 nm (formed by random creation of Cl vacancies *via* electron-simulated desorption),[42] in line with the here observed trend. Our well-controllable lateral manipulation technique provides novel opportunities to monitor the coupling of IS with the attractive potential associated with the vacancy during the formation of dimers with different separation distances.

CONCLUSIONS

In conclusion, using scanning tunneling microscopy we demonstrate lateral manipulation of Cl vacancies in bilayer NaCl on Au(111), allowing the formation of vacancy dimers as well as larger nanostructures consisting of multiple vacancies. We find that the coupling of the interface state with an individual Cl vacancy, as well as the coupling of the vacancy state of the individual Cl vacancy to the optical phonons in the NaCl film, can be modified by bringing a second vacancy nearby, thereby creating a vacancy dimer. The lateral repositioning of atomic vacancies opens up a new playground for investigation of fundamental physical properties of vacancy nanostructures of any desired size and shape and their coupling with the supporting substrate, as well as the interaction of various deposits with charged vacancies. The control of the density and the nature of vacancies may provide a means for tailoring the surface reactivity.[43,44]

METHODS

NaCl layers are grown using vapor deposition at 800 K in the preparation chamber of an STM setup (Oxford Instruments−Omicron NanoScience) under ultrahigh vacuum (UHV) conditions. 1L, 2L, and 3L NaCl(100) islands are prepared as described in refs 38 and 45. (d*I*/d*V*)(*V*) curves and maps are acquired with an open or closed feedback loop by lock-in detection using a modulation

amplitude of 10 mV at 888 Hz. All STM measurements are performed in UHV (10^{-11} mbar) and at low temperature (T_{sample} = 4.5 K). Image processing is performed by Nanotec WSxM.[46] All voltages refer to the sample bias with respect to the STM tip.

Spin-polarized DFT calculations were performed using the generalized gradient approximation (PBE functional)[47] and the plane waves code VASP.[48,49] The interaction between the ions and the valence electrons is described by the projector augmented wave (PAW) method.[50] The NaCl(100) films on the Au(111) substrate have been modeled by a coincidence structure, obtained by superposing a (4 × 4) NaCl(100) unit cell on a $\begin{pmatrix} 1 & 3 \\ 3 & 1 \end{pmatrix}$ superstructure of the Au(111) surface.[51,52] The metal support is modeled by a five-layer slab. Fourteen angstroms of empty space is included to avoid spurious interactions between the replicas of the slab model. The Γ point is used for the reciprocal space sampling. Dispersion interactions are included by means of the pairwise force field as implemented by Grimme (DFT-D2).[53] STM images are simulated using the Tersoff–Hamann approximation.[54] Concerning the location of transition states, the use of constrained optimization and of the dimer method[32] are applied. For the former a Cl atom is placed above the surface (0.5–2.0 Å) between two nearest-neighbor Cl vacancies and the geometries are optimized while fixing the Cl atom above the surface. The dimer method is based on the first derivative of the potential energy and drives the geometry optimization to convergence to a saddle point instead of to a minimum.

Conflict of Interest: The authors declare no competing financial interest.

Acknowledgment. This research has been supported by the Research Foundation–Flanders (FWO, Belgium), the Flemish Concerted Action (BOF KU Leuven, Project No. GOA/14/007) research program, and the Italian MIUR (FIRB Project No. RBAP115AYN). Z.L. thanks the China Scholarship Council for financial support (No. 2011624021). K.S. acknowledges support from the FWO.

Supporting Information Available: Formation of nanostructures composed of multiple Cl vacancies; height profile of Cl vacancies at high tunneling voltage; atomic scale structure and partial charge density of Cl vacancies. This material is available free of charge *via* the Internet at http://pubs.acs.org.

REFERENCES AND NOTES

1. Kittel, C. *Introduction to Solid State Physics*, 8th ed.; Wiley: New York, 2005.
2. Oba, F.; Choi, M.; Togo, A.; Tanaka, I. Point Defects in ZnO: An Approach from First Principles. *Sci. Technol. Adv. Mater.* **2011**, *12*, 034302.
3. Feng, Z. A.; El Gabaly, F.; Ye, X.; Shen, Z. X.; Chueh, W. C. Fast Vacancy-Mediated Oxygen Ion Incorporation across the Ceria-Gas Electrochemical Interface. *Nat. Commun.* **2014**, *5*, 4374.
4. Stengel, M.; Vita, A. D.; Baldereschi, A. Adatom-Vacancy Mechanisms for the C_{60}/Al(111)-(6×6) Reconstruction. *Phys. Rev. Lett.* **2003**, *91*, 166101.
5. Hynninen, T.; Cabailh, G.; Foster, A. S.; Barth, C. Defect Mediated Manipulation of Nanoclusters on an Insulator. *Sci. Rep.* **2013**, *3*, 1270.
6. Pacchioni, G.; Freund, H. Electron Transfer at Oxide Surfaces. The MgO Paradigm: From Defects to Ultrathin Films. *Chem. Rev.* **2013**, *113*, 4035–4072.
7. Chao, K. J.; Smith, A. R.; Shih, C. K. Direct Determination of Exact Charge States of Surface Point Defects Using Scanning Tunneling Microscopy: As Vacancies on GaAs (110). *Phys. Rev. B* **1996**, *53*, 6935–6938.
8. Sanchez, A.; Abbet, S.; Heiz, U.; Schneider, W. D.; Häkkinen, H.; Barnett, R. N.; Landman, U. When Gold Is Not Noble: Nanoscale Gold Catalysts. *J. Phys. Chem. A* **1999**, *103*, 9573–9578.
9. Yoon, B.; Häkkinen, H.; Landman, U.; Wörz, A. S.; Antonietti, J.-M.; Abbet, S.; Judai, K.; Heiz, U. Charging Effects on Bonding and Catalyzed Oxidation of CO on Au_8 Clusters on MgO. *Science* **2005**, *307*, 403–407.
10. Jensen, H.; Kröger, J.; Berndt, R.; Crampin, S. Electron Dynamics in Vacancy Islands: Scanning Tunneling Spectroscopy on Ag(111). *Phys. Rev. B* **2005**, *71*, 155417.
11. Rodary, G.; Sander, D.; Liu, H.; Zhao, H.; Niebergall, L.; Stepanyuk, V. S.; Bruno, P.; Kirschner, J. Quantization of the Electron Wave Vector in Nanostructures: Counting *k*-States. *Phys. Rev. B* **2007**, *75*, 233412.
12. Sterrer, M.; Heyde, M.; Novicki, M.; Nilius, N.; Risse, T.; Rust, H.-P.; Pacchioni, G.; Freund, H.-J. Identification of Color Centers on MgO(001) Thin Films with Scanning Tunneling Microscopy. *J. Phys. Chem. B* **2006**, *110*, 46–49.
13. Repp, J.; Fölsch, S.; Meyer, G.; Rieder, K.-H. Ionic Films on Vicinal Metal Surfaces: Enhanced Binding Due to Charge Modulation. *Phys. Rev. Lett.* **2001**, *86*, 252–255.
14. Li, Z.; Schouteden, K.; Iancu, V.; Janssens, E.; Lievens, P.; Van Haesendonck, C.; Cerda, J. I. Chemically Modified STM Tips for Atomic-Resolution Imaging on Ultrathin NaCl Films. *Nano Res.* **2015**, in press.
15. Schouteden, K.; Lauwaet, K.; Janssens, E.; Barcaro, G.; Fortunelli, A.; Van Haesendonck, C.; Lievens, P. Probing the Atomic Structure of Metallic Nanoclusters with the Tip of a Scanning Tunneling Microscope. *Nanoscale* **2014**, *6*, 2170–2176.
16. Repp, J.; Meyer, G.; Paavilainen, S.; Olsson, F. E.; Persson, M. Scanning Tunneling Spectroscopy of Cl Vacancies in NaCl Films: Strong Electron-Phonon Coupling in Double-Barrier Tunneling Junctions. *Phys. Rev. Lett.* **2005**, *95*, 225503.
17. Steurer, W.; Gross, L.; Meyer, G. Local Thickness Determination of Thin Insulator Films *via* Localized States. *Appl. Phys. Lett.* **2014**, *104*, 231606.
18. Tong, X.; Wolkow, R. A. Electron-Induced H Atom Desorption Patterns Created with a Scanning Tunneling Microscope: Implications for Controlled Atomic-Scale Patterning on H–Si(100). *Surf. Sci.* **2006**, *600*, L199–L203.
19. Schofield, S. R.; Studer, P.; Hirjibehedin, C. F.; Curson, N. J.; Aeppli, G.; Bowler, D. R. Quantum Engineering at the Silicon Surface Using Dangling Bonds. *Nat. Commun.* **2013**, *4*, 1649.
20. Livadaru, L.; Xue, P.; Shaterzadeh-Yazdi, Z.; DiLabio, G. A. Mutus, J.; Pitters, J. L.; Sanders, B. C.; Wolkow, R. A. Dangling-Bond Charge Qubit on a Silicon Surface. *New J. Phys.* **2010**, *12*, 083018.
21. Ferng, S.-S.; Lin, D.-S. Iodine Adsorption on Arrays, Clusters, and Pairs of Reactive Sites on the Si(100) Surface. *J. Phys. Chem. C* **2012**, *116*, 3091–3096.
22. Li, H.-D.; Chang, C.-Y.; Chien, L.-Y.; Chang, S.-H.; Chiang, T. C.; Lin, D.-S. Adsorption and Abstraction Reactions of HCl on a Single Si(100) Dangling Bond. *Phys. Rev. B* **2011**, *83*, 075403.
23. Eigler, D. M.; Schweizer, E. K. Positioning Single Atoms with a Scanning Tunnelling Microscope. *Nature* **1990**, *344*, 524–526.
24. Bartels, L.; Meyer, G.; Rieder, K. H. Basic Steps of Lateral Manipulation of Single Atoms and Diatomic Clusters with a Scanning Tunneling Microscope Tip. *Phys. Rev. Lett.* **1997**, *79*, 697–700.
25. Stipe, B. C.; Rezaei, M. A.; Ho, W. Site-Specific Displacement of Si Adatoms on Si(111)-(7×7). *Phys. Rev. Lett.* **1997**, *79*, 4397–4400.
26. Dujardin, G.; Mayne, A.; Robert, O.; Rose, F.; Joachim, C.; Tang, H. Vertical Manipulation of Individual Atoms by a Direct STM Tip-Surface Contact on Ge(111). *Phys. Rev. Lett.* **1998**, *80*, 3085–3088.
27. Gimzewski, J. K.; Joachim, C. Nanoscale Science of Single Molecules Using Local Probes. *Science* **1999**, *283*, 1683–1688.
28. Swart, I.; Sonnleitner, T.; Niedenführ, J.; Repp, J. Controlled Lateral Manipulation of Molecules on Insulating Films by STM. *Nano Lett.* **2012**, *12*, 1070–1074.
29. Kawai, S.; Foster, A. S.; Canova, F. F.; Onodera, H.; Kitamura, S.; Meyer, E. Atom Manipulation on an Insulating Surface at Room Temperature. *Nat. Commun.* **2014**, *5*, 4403.
30. Trevethan, T.; Watkins, M.; Kantorovich, L. N.; Shluger, A. L. Controlled Manipulation of Atoms in Insulating Surfaces

with the Virtual Atomic Force Microscope. *Phys. Rev. Lett.* **2007**, *98*, 028101.
31. Hebenstreit, W.; Redinger, J.; Horozova, Z.; Schmid, M.; Podloucky, R.; Varga, P. Atomic Resolution by STM on Ultra-Thin Films of Alkali Halides: Experiment and Local Density Calculations. *Surf. Sci.* **1999**, *424*, L321–L328.
32. Henkelman, G.; Jónsson, H. A Dimer Method for Finding Saddle Points on High Dimensional Potential Surfaces Using Only First Derivatives. *J. Chem. Phys.* **1999**, *111*, 7010–7022.
33. Girard, C.; Joachim, C.; Chavy, C.; Sautet, P. The Electric Field under a STM Tip Apex: Implications for Adsorbate Manipulation. *Surf. Sci.* **1993**, *282*, 400–410.
34. Dougherty, D. B.; Maksymovych, P.; Lee, J.; Feng, M.; Petek, H.; Yates, J. T. Tunneling Spectroscopy of Stark-Shifted Image Potential States on Cu and Au Surfaces. *Phys. Rev. B* **2007**, *76*, 125428.
35. Ploigt, H.-C.; Brun, C.; Pivetta, M.; Patthey, F.; Schneider, W.-D. Local Work Function Changes Determined by Field Emission Resonances: NaCl/Ag(100). *Phys. Rev. B* **2007**, *76*, 195404.
36. Suich, D. E.; Caplins, B. W.; Shearer, A. J.; Harris, C. B. Femtosecond Trapping of Free Electrons in Ultrathin Films of NaCl on Ag(100). *J. Phys. Chem. Lett.* **2014**, *5*, 3073–3077.
37. Pavliček, N.; Swart, I.; Niedenführ, J.; Meyer, G.; Repp, J. Symmetry Dependence of Vibration-Assisted Tunneling. *Phys. Rev. Lett.* **2013**, *110*, 136101.
38. Lauwaet, K.; Schouteden, K.; Janssens, E.; Van Haesendonck, C.; Lievens, P. Dependence of the NaCl/Au(111) Interface State on the Thickness of the NaCl Layer. *J. Phys.: Condens. Matter* **2012**, *24*, 475507.
39. Olsson, F. E.; Persson, M.; Borisov, A. G.; Gauyacq, J. P.; Lagoute, J.; Fölsch, S. Localization of the Cu(111) Surface State by Single Cu Adatoms. *Phys. Rev. Lett.* **2004**, *93*, 206803.
40. Limot, L.; Pehlke, E.; Kröger, J.; Berndt, R. Surface-State Localization at Adatoms. *Phys. Rev. Lett.* **2005**, *94*, 036805.
41. Schouteden, K.; Lievens, P.; Van Haesendonck, C. Low-Temperature STM/STS Investigation of Nanostructures Created by an STM Tip on Au(111) Surfaces. *Appl. Phys. A: Mater. Sci. Processes* **2009**, *96*, 409–413.
42. Repp, J. Rastertunnelmikroskopie und -Spektroskopie an Adsorbaten auf Metall- und Isolatoroberflächen. *Thesis at the Freie University of Berlin*, 2002.
43. Campbell, C. T.; Peden, C. H. F. Oxygen Vacancies and Catalysis on Ceria Surfaces. *Science* **2005**, *309*, 713–714.
44. Esch, F.; Fabris, S.; Zhou, L.; Montini, T.; Africh, C.; Fornasiero, P.; Comelli, G.; Rosei, R. Electron Localization Determines Defect Formation on Ceria Substrates. *Science* **2005**, *309*, 752–755.
45. Schouteden, K.; Li, Z.; Iancu, V.; Muzychenko, D. A.; Janssens, E.; Lievens, P.; Van Haesendonck, C. Engineering the Band Structure of Nanoparticles by an Incommensurate Cover Layer. *J. Phys. Chem. C* **2014**, *118*, 18271–18277.
46. Horcas, I.; Fernandez, R.; Gomez-Rodriguez, J. M.; Colchero, J.; Gomez-Herrero, J.; Baro, A. M. Wsxm: A Software for Scanning Probe Microscopy and a Tool for Nanotechnology. *Rev. Sci. Instrum.* **2007**, *78*, 013705–8.
47. Perdew, J. P.; Burke, K.; Ernzerhof, M. Generalized Gradient Approximation Made Simple. *Phys. Rev. Lett.* **1996**, *77*, 3865–3868.
48. Kresse, G.; Hafner, J. *Ab Initio* Molecular Dynamics for Liquid Metals. *Phys. Rev. B* **1993**, *47*, 558–561.
49. Kresse, G.; Furthmüller, J. Efficient Iterative Schemes for *ab Initio* Total-Energy Calculations Using a Plane-Wave Basis Set. *Phys. Rev. B* **1996**, *54*, 11169–11186.
50. Blöchl, P. E. Projector Augmented-Wave Method. *Phys. Rev. B* **1994**, *50*, 17953–17979.
51. Lauwaet, K.; Schouteden, K.; Janssens, E.; Van Haesendonck, C.; Lievens, P.; Trioni, M. I.; Giordano, L.; Pacchioni, G. Resolving All Atoms of an Alkali Halide *via* Nanomodulation of the Thin NaCl Film Surface Using the Au(111) Reconstruction. *Phys. Rev. B* **2012**, *85*, 245440.
52. Li, Z.; Chen, H. Y. T.; Schouteden, K.; Lauwaet, K.; Giordano, L.; Trioni, M. I.; Janssens, E.; Iancu, V.; Van Haesendonck, C.; Lievens, P.; *et al*. Self-Doping of Ultrathin Insulating Films by Transition Metal Atoms. *Phys. Rev. Lett.* **2014**, *112*, 026102.
53. Grimme, S. Semiempirical GGA-Type Density Functional Constructed with a Long-Range Dispersion Correction. *J. Comput. Chem.* **2006**, *27*, 1787–1799.
54. Tersoff, J.; Hamann, D. R. Theory of the Scanning Tunneling Microscope. *Phys. Rev. B* **1985**, *31*, 805–813.